




Cluster analysis reveals patterns of age-related change in anterior chamber depth for gender and ethnicity: clinical implications

Jack Phu^{1,2} , Janelle Tong^{1,2} , Barbara Zangerl^{1,2} , Janet Ly Le^{1,2} and Michael Kalloniatis^{1,2} 

¹Centre for Eye Health, University of New South Wales, Kensington, NSW, Australia, and ²School of Optometry and Vision Science, University of New South Wales, Kensington, NSW, Australia

Citation information: Phu J, Tong J, Zangerl B, Le JL, & Kalloniatis M. Cluster analysis reveals patterns of age-related change in anterior chamber depth for gender and ethnicity: clinical implications. *Ophthalmic Physiol Opt* 2020; 40: 632–649. <https://doi.org/10.1111/opo.12714>

Keywords: angle closure, angle closure disease, glaucoma, narrow angles, Pentacam, Scheimpflug imaging

Correspondence: Jack Phu
E-mail address: jphu@cfh.com.au

Received: 9 April 2020; Accepted: 28 May 2020; Published online: 9 July 2020

Financial support

Guide Dogs NSW/ACT provides funding for clinical services delivered at the Centre for Eye Health, where the patient data was collected. JP, JT, BZ and MK all receive salary support from Guide Dogs NSW/ACT. JLL was supported by a Summer Vacation Research Scholarship funded by Guide Dogs NSW/ACT. The funding body played no role in the conception or conduct of the study.

Abstract

Purpose: To identify patterns of age-, gender- and refractive- related changes in Scheimpflug-based anterior chamber depth across the central 8 mm of chamber width, to derive normative models, potentially useful for angle closure disease diagnosis.

Methods: This was a retrospective, cross-sectional study. Scheimpflug photography was used to obtain anterior chamber depth measurements at 57 points across the central 8 mm of the chamber width from one eye of each healthy subject (male Caucasians ($n = 189$), female Caucasians ($n = 186$), male Asians ($n = 165$) and female Asians ($n = 181$)). Sliding window and nonlinear regression analysis was used to identify the age-related changes in chamber depth. Hierarchical cluster analysis was used to identify test locations with statistically identical age-related shifts, which were used to perform age-correction for all subjects, resulting in normative distributions of chamber depth across the chamber width. The model was examined with and without the contribution of spherical equivalent refractive error.

Results: Distinct clusters, demonstrating statistically indistinguishable age-related changes of chamber depth over time, were identified. These age-related changes followed a nonlinear regression (fifth or sixth order polynomial). Females tended to have a greater rate of chamber depth shallowing. Incorporating refractive error into the model produced minimal changes to the fit relative to the ground truth. Comparisons with cut-offs for angle closure from the literature showed that ageing alone was insufficient for identifying angle closure disease.

Conclusions: Age-, ethnicity- and gender-related differences need to be acknowledged in order to utilise anterior chamber depth data for angle closure disease diagnosis correctly. Ageing alone does not adequately account for the angle closure disease process.

1. Introduction

Glaucoma is one of the leading causes of irreversible blindness worldwide.^{1–3} Although the open-angle form is generally more common in most health care settings, angle closure glaucoma is typically associated with greater rates of blindness, especially in Asian populations⁴ and amongst females.⁵ The current gold standard for diagnosis and

staging of angle closure spectrum disease uses gonioscopy.⁶ This technique is skill intensive and can be fairly invasive, requiring the instillation of anaesthetic drops, and is burdened by the subjectivity regarding the interpretation of the results.⁷

As a means to address some of the limitations of gonioscopy, non-invasive imaging modalities designed to examine the anterior segment have been suggested as

complementary techniques to provide additional qualitative or quantitative information.⁸ Specifically, methods obtaining quantitative information may be more conducive to telemedicine or virtual clinic approaches due to their potentially less ambiguous findings relative to gonioscopy.⁹ Scheimpflug imaging is one example of a non-invasive technique for assessing anterior chamber parameters.¹⁰

Applications of Scheimpflug photography for angle closure spectrum disease reported in the literature have primarily exploited singular anterior chamber depth, angle and volume parameters.^{11–14} These parameters offer a simple method for assessing the risk of angle closure. However, there are several questions remaining regarding their use. Unlike parameters such as visual field data and retinal thickness, Scheimpflug-derived data and their instrument outputs do not typically account for age- or gender-related factors, despite known differences occurring with both factors.^{15–20} Importantly, advancing age, Asian ethnicity and female gender are associated with increased rates of angle closure.^{21,22} Therefore, the question remains: how do age-, ethnicity- or gender-related changes impact upon the ability of these parameters to correctly identify patients with or at risk of developing disease? Currently, the paracentral region is largely ignored. Anterior chamber depth typically becomes shallower in the periphery, but it is not yet known whether patterns of equal chamber depth exist across the chamber width. If areas of equal depth (iso-depth) exist, we hypothesise that measurement variability would reduce, leading to identification of anterior chamber depth measurements that would be able to stratify patients at risk of angle closure.

In the present study, we leveraged our recently developed and applied cluster analysis techniques^{23–27} to examine these issues. We used Scheimpflug photography to obtain central and paracentral anterior chamber depth information from a normal cohort spanning a wide range of ages in males and females of both Caucasian and Asian ethnicities. We applied cluster analysis to identify regions sharing similar age-related changes and characterised these using non-linear regression. Then, we performed age-correction to obtain normative distributions of anterior chamber depths for application in the examination of angle closure disease. Since some studies have suggested an effect of refractive error on chamber depth,^{17,18,28} we also examined a model incorporating spherical equivalent refractive error.

2. Methods

2.1. Subjects

All subjects provided written informed consent. The study adhered to the Declaration of Helsinki and ethics approval was provided by the Human Research Ethics Committee of the University of New South Wales, Australia.

All subject data were retrospectively collected from the files of patients seen at the Centre for Eye Health (CFEH), University of New South Wales. All patients had undergone comprehensive examination at the CFEH following a referral from their primary eye care practitioner, which could have been for a diverse range of reasons; we were careful to screen for normality as per the eligibility criteria described below. All eligible subjects had undergone Scheimpflug imaging using the Pentacam HR (www.oculus.de/en/products/tomography/pentacam-pentacam-hr-pentacam-axl/). Subjects comprised a retrospective cohort of healthy individuals who all had normal eye examination findings: i.e., best corrected visual acuity of 6/7.5 or better (6/10 or better for subjects over age 60) and age-normal anterior and posterior ocular health as assessed by slit lamp examination supplemented by imaging modalities such as optical coherence tomography of the macula and optic nerve. Subjects with primary angle closure suspect status or worse (defined as 2+ quadrants where the posterior trabecular meshwork could not be seen) were excluded. This was ruled out using a combination of Van Herick limbal anterior chamber depth measurement, gonioscopy, and anterior segment optical coherence tomography. Subjects with glaucoma or intraocular pressure >21 mmHg were excluded. Patients with cataracts were included if they were not visually significant (by the acuity criteria listed above). No subjects had a history of systemic disease known to affect the cornea or anterior segment. Subjects were divided by self-reported gender and ethnicity. Specifically, we were interested in patients of Caucasian and East Asian (henceforth simplified to 'Asian') descent, with the total number of subjects being 189, 186, 165 and 181 male Caucasians, female Caucasians, male Asians and female Asians, respectively (Table 1).

2.2. Data extraction

Anterior chamber data were extracted from one randomly selected eye from the total cohort. A random eye was selected to avoid potential systematic biases such as one eye being more accurately measured than the other by the technicians in the clinic. Although this may mask some of the systematic trends seen on a per-eye basis, it is more likely that in the normal eye, biometric parameters may be largely similar.²⁹

Data were exported using the Pentacam software version 6.08r27 (www.pentacam.com/int/models/software-ao0.html), which provided individual datum points in a 4 mm radius from the optical centre at 0.1 mm intervals (>5000 points). Using these data points, we calculated the anterior chamber depth at the locations corresponding to the 57 test points typically reported in the Pentacam anterior chamber depth printout across the central 8 mm of chamber width using a custom written macro on Microsoft Excel 2010

Table 1. Demographics of subjects within the present study

| | | Male Caucasians | Female Caucasians | Male Asians | Female Asians |
|---------------------------------|---------------------|-----------------|-------------------|--------------|---------------|
| Number of subjects (<i>n</i>) | | 189 | 186 | 165 | 181 |
| Refractive error (diopetre) | Median | -0.13 | 0.00 | -1.13 | -1.13 |
| | Interquartile range | -1.50, +0.50 | -0.72, +0.75 | -3.38, 0.00 | -3.75, +0.13 |
| | Range | -6.38, +5.50 | -7.75, +5.50 | -8.50, +2.63 | -8.25, +5.13 |
| Age (<i>n</i>) | <10 | 5 | 4 | 3 | 2 |
| | 10 to <20 | 23 | 20 | 20 | 19 |
| | 20 to <30 | 30 | 26 | 27 | 39 |
| | 30 to <40 | 31 | 23 | 20 | 26 |
| | 40 to <50 | 27 | 28 | 25 | 26 |
| | 50 to <60 | 27 | 28 | 30 | 33 |
| | 60 to <70 | 23 | 25 | 27 | 27 |
| | 70 to <80 | 21 | 27 | 12 | 9 |
| | 80+ | 2 | 5 | 1 | 0 |

(www.microsoft.com).²⁵ These points are arranged in rings of 1 mm interval radii up to 4 mm from the optical centre. One eye from each subject was selected at random for inclusion in the study.

2.3. Age-related changes in anterior chamber depth across the chamber width – sliding window analysis

To determine age-related changes in anterior chamber depth, we firstly organised the data from all subjects into smaller groups. To mitigate potential biases arising from arbitrary decade-based grouping (e.g. ≤10 years, 11–20 years, 21–30 years, etc.) we used a sliding window procedure. The sliding window technique overcomes issues regarding sampling density and arbitrarily defined brackets.^{25,30} In this, we sequentially added one year to each age bracket, maintaining the same 10-year span, but effectively shifting the bracket centre to obtain a range of samples not limited to the arbitrary decade-based groups (e.g. 11–20, 12–21, 13–22, etc.). Each window represented a single mean ‘age’ contributing a depth value for each location, and these were used as the groups for cluster analysis to identify locations with the same age-related change. For the windows with sparse sampling or gaps (e.g. ages 53–58 years) in the female Asian cohort, we generated additional smaller windows (5-year increments) for analysis, and this did not change the results of the analysis.

2.4. Age-related changes in anterior chamber depth across the chamber width – cluster analysis

Clustering for identifying locations with the same age-related depth change was performed using hierarchical agglomerative clustering (within groups linkage and squared Euclidean distance) on SPSS Statistics Version 25.0 (<https://www.ibm.com/analytics/spss-statistics-software>).

In brief, hierarchical clustering utilises an agglomerative technique to group statistically similar measurements from individual points into successively large clusters, eventually into the total cohort. Hierarchical agglomerative clustering was chosen as it effectively facilitates a ‘bottom-up’ approach, in comparison to the ‘top-down’ approach of K-means clustering.³¹ In K-means, the number of clusters expected to arise from the clustering should be known; given that there is little historical precedent, hierarchical clustering allowed for greater granularity when exploring our data. In comparison to other models such as Gaussian mixture modelling, we also wished to visualise the complete hierarchy and have an algorithm that was relatively insensitive to the distance metric.

Another potential clustering method is Gaussian mixture models. Although this method accounts for the variance within each cluster similar to hierarchical clustering, it also requires the number of clusters to be initially known, like K-means. A key advantage of Gaussian mixture models is that it returns probabilities that a data point belongs within a specific cluster. However, this was not the purpose of our study, and hence was not deployed on our data set. Instead, our purpose was to assess the normality of the resultant distribution of depths within each cluster that would then allow the derivation of normative distributions (see further below).

In this study, cases were labelled using their position within the map of the cornea, but spatial information was not used for the clustering method (i.e. no assumptions regarding spatial arrangement of the resultant clusters are made *a priori*). Applied here, clustering allowed us to identify test locations across the chamber width that exhibit the statistically similar age-related change. In doing so, we could then group those test locations to create robust models describing the age-related changes. Different stages of merging can be visualised using the resultant dendrogram.

For the identification of age-related clusters, we did not use the amalgamation schedule, but rather took the first branch of the dendrogram, which returns the maximum number of output clustered groups, all of which were initially retained. The separation and differences between groups were assessed as per the methods described below.

Mean anterior chamber depths at each location were plotted as a function of mean age for each window as described above, and were fitted with linear and polynomial curves to determine the best fit, as assessed using an *F*-test for comparing function fit, the coefficient of determination, R^2 and Bland-Altman analysis. We chose to use the extra sum-of-squares *F*-test for comparing function fits, and to determine whether a single function was optimal for fitting each group of data (for example when comparing identified clusters within a cohort, or comparing similar across cohorts), rather than other information criteria (such as Akaike's information criteria). This was because the overall null hypothesis was that a single function would adequately fit all of the 'population' data. Hence, a rejection of this null hypothesis using the *F*-test would suggest that different conditions (such as different clusters or cohorts) would be better described using different age-related functions.

2.5. Determining age-corrected normative distributions of anterior chamber depth

Age-correction factors were derived from the functions described above, and then reapplied to the cohort's data, in order to age-correct all subjects' depth results to a 35-year-old equivalent subject (due to the propensity for a greater number of subjects with reliable data to occur within this age-group). The age-corrected results (minus the 30 to 40-year-old group) were then compared with the depth values obtained from the 30 to 40-year-old decade group for each respective cohort separately; this formed the ground truth, using Bland-Altman plots. Note that we further tested the other decade-brackets (e.g. mean 15-, 25-, 45- etc year-old equivalent) and evaluated their levels of agreement against their respective ground truth cohorts using the Bland-Altman method; see Results for further details.

Due to the nature of the sliding window analysis providing mean ages as data points for the regression analysis, we limited the comparison between ground truth and derived age-corrected cohort to subjects within the age range of the sliding windows. For example, if the mean ages of the windows ranged between 11 and 65 years old, then the age-correction and comparisons with the ground truth would only be performed on subjects within that range (minus the 30 to 40-year-old comparator group).

Following determination of the optimal age-correction for each condition, we again performed cluster analysis as

described above to determine the age-corrected iso-depth contours for anterior chamber depth. These iso-depth contours facilitated grouping of test locations together to obtain a final age-corrected, normative distribution for each location across the chamber width.

In addition to referring to the dendrogram breaks, we also used a systematic approach to merge the clusters, as these all represented a unified 35-year-old equivalent subject based on the separability of the clusters. Separability analysis was performed using the d' statistic, as per our previous methods (Equation 1).^{23,24} Clusters were systematically merged, starting with the cluster pair with the lowest d' value, until all comparisons had a $d' > 1$. Members within each cluster therefore indicated test locations that shared sufficiently similar distribution characteristics within 1 standard deviation unit.

$$d' = \frac{|x_1 - x_2|}{\sqrt{0.5 \times (\sigma_1^2 + \sigma_2^2)}} \quad (1)$$

The distributions of anterior chamber depths were assessed using the D'Agostino and Pearson K^2 test of normality (where $p < 0.05$ indicated a rejection of normality of distribution; this test of normality is similar to Shapiro-Wilk for long-tailed distributions, which was our prediction with this data set³²), and Gaussian or non-Gaussian statistics, as appropriate.

2.6. Effect of spherical equivalent refractive error

We also examined the relationship between spherical equivalent refractive error and anterior chamber depth prior to, and following, age-correction for each cohort. In this analysis, we performed regression analysis using spherical equivalent refractive error and pointwise anterior chamber depths. Extra sums-of-squares *F*-tests were used to determine differences in slope and intercepts from the regression analysis. After determining refractive error related changes, we applied refraction correction to determine the effects of age and age-corrected depth distributions, and compared the cluster patterns to the models without refraction correction described above.

2.7. Clinical applications: using normative distributions of chamber depth for assessing angle closure spectrum disease

Several papers have provided cut-off values of anterior chamber quantitative parameters for the purposes of screening for angle closure spectrum disease using Scheimpflug imaging. Some studies have reported good ability of Scheimpflug imaging to distinguish between open and narrow angles,^{12,33-36} while others have been more

reserved.^{37,38} Notably, the cut-off values for central anterior chamber depth supplied by each study vary significantly from as low as 1.93 mm by Rossi *et al.*³⁴ to 2.58 mm by Kurita *et al.*¹⁴

We aimed to assess each of these cut-off values using our age-corrected cohorts. We extracted the mean age and cut-off angle closure, disease and central anterior chamber depth values from each study. Using the mean age for each study, we calculated the equivalent anterior chamber distributions for an age-corrected normal subject. Then, the percentile ranking of the cut-off value relative to the normal distribution was calculated using *Z*-scores. These were assessed using normative distributions for each gender and ethnicity combination.

2.8. Statistical analyses

Statistical analyses were performed using GraphPad Prism version 8 (<https://www.graphpad.com/scientific-software/prism/>) and SPSS Statistics version 25 for Mac. Specific analyses are described in the above text, and further to this, comparisons of the results by each gender were performed using unpaired *t*-tests (for the distribution of anterior chamber depth measurements) and extra sum-of-squares *F* test (for the functions used to fit the age-related changes, including within-cohort, between-cluster functions, and between-cohort, within-cluster functions).

3. Results

3.1. Age-related changes in anterior chamber depth across the chamber width

Cluster analysis applied to determining age-related changes in anterior chamber depth identified seven different clusters for each of the four cohorts, with similar asymmetric concentricity of the patterns across the chamber width (Figure 1). As detailed in the method section, the resultant clusters were the maximum number of output cluster groups identified using the bottom-up hierarchical approach (i.e. no grouping was performed prior to this analysis step).

Regression analysis applied to the sliding window grouped data for each of the seven clusters identified a tendency for chamber depth to peak slightly in the teenage years, before undergoing a downward trend with age. For male and female Caucasian groups, a centred sixth-order polynomial offered the best fit to the data, whilst for male and female Asian groups, the best fit was dependent on location, which was either a fifth or sixth order polynomial (Table 2). The second derivative differential (d^2y/dx^2) showed that the greatest rate of change occurred in the mid-20s. The other solution to the second derivative was

approximately 9 years of age, but this was confounded by the small sampling at that age group.

Extra sum-of-squares *F*-test conducted within each cohort found significant differences in the age-related change across each identified cluster ($p < 0.0001$). The large number of mutual points across groups 1–7 allowed us to perform within-group analysis comparing the gender and ethnicity cohorts. The sum-of-squares *F*-test found significant differences between gender and slight differences between ethnicity ($p < 0.0001$). In combination, these provided additional support for the separation of classes using cluster analysis.

3.2. Age-corrected distributions of anterior chamber depth across the chamber width

Age-correction factors obtained from the above analyses were applied to each cohort to convert all individuals into a 35-year-old equivalent subject. Cluster analysis applied to the age-corrected cohort identified four resultant clusters of iso-depth across the chamber width for each cohort (separated by d -prime > 1) (Figure 2). The patterns of iso-depth approximated an asymmetric, concentric pattern (Table 3). Tests of normality were conducted for each cluster and none was found to be statistically significant, and therefore the mean and standard deviations could be used to infer the normal distribution limits from the totality of the normal cohort (Table 4).

Using age-corrected depths, one-way analysis of variance (ANOVA) showed significant differences in chamber depth across each cohort, i.e. group 1 was different in terms of their distribution characteristics ($p < 0.0001$). Multiple comparisons showed that these differences were only significant for male versus female cohorts, but not for male Caucasian versus male Asian or for female Caucasian versus female Asian groups.

3.3. Agreement with the ground truth

Bland-Altman analyses (in percentages, to facilitate comparisons across different depths and cohorts) comparing age-corrected with ground truth anterior chamber depths are shown in Figure 3. More central test locations exhibited smaller differences between ground truth and age-corrected depths. Peripheral locations, particularly superiorly, showed greater differences across all cohorts.

We then assessed the agreement with the ground truth across second- to sixth-order polynomials and linear fits to the sliding window data; this was performed for five decade brackets (20–30 to 60–70 years). The resultant Bland-Altman analyses showed small differences in overall mean bias, whereby no regression produced a biased result. The differences between polynomial fits

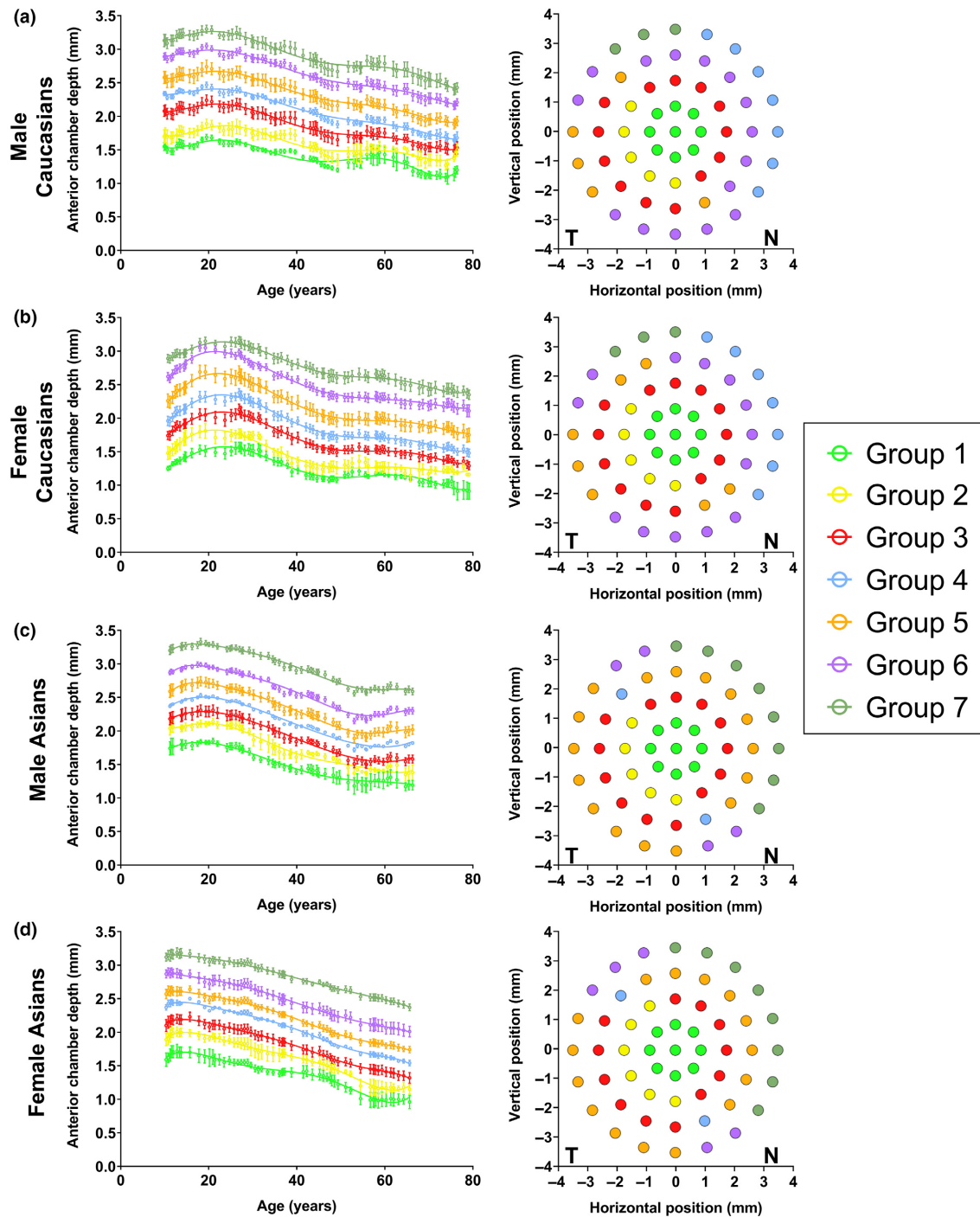


Figure 1. Analysis of age-related changes in anterior chamber depth (mm) across the four cohorts in the present study (rows a–d). Left: nonlinear regression analysis plotting depth (mm) as a function of age (years). Polynomial fits are shown in Table 2. Each datum point represents a subgroup of subjects within a 10-year window of ages, with the range of points demonstrating the sliding window analysis. Error bars indicate one standard deviation. Each colour on the left panel corresponds to the same coloured cluster on the right hand side maps. Right: theme maps representing groups of test locations demonstrating statistically identical rates of chamber depth changes found using hierarchical cluster analysis. The axes indicate the physical position of the test location (N, nasal; T, temporal).

Table 2. Best-fit polynomial functions for each cohort divided by each of the seven clusters from hierarchical cluster analysis (Figure 1)

| Male Caucasians | | | | | | | |
|-------------------|-------------|-------------|-------------|-------------|-------------|-------------|-------------|
| Cluster | 1 | 2 | 3 | 4 | 5 | 6 | 7 |
| B0 | 1.338 | 1.537 | 1.818 | 2.07 | 2.308 | 2.609 | 2.849 |
| B1 | -0.007046 | -0.01404 | -0.01682 | -0.01776 | -0.01735 | -0.01873 | -0.01721 |
| MeanX | 42.5 | 42.5 | 42.5 | 42.5 | 42.5 | 42.5 | 42.5 |
| B2 | 0.001194 | 0.000991 | 0.0007876 | 0.000512 | 0.0006374 | 0.0005719 | 0.0008644 |
| B3 | -3.9E-06 | 1.3E-05 | 1.1E-05 | 1.2E-05 | 8.1E-06 | 1.1E-05 | 9.9E-06 |
| B4 | -2.6E-06 | -2.2E-06 | -1.6E-06 | -1.1E-06 | -1.4E-06 | -1.1E-06 | -1.6E-06 |
| B5 | 4.2E-09 | -4.2E-09 | -3.3E-09 | -4.2E-09 | -1.1E-09 | -3.7E-09 | -3.5E-09 |
| B6 | 1.4E-09 | 1.2E-09 | 8.0E-10 | 5.3E-10 | 6.8E-10 | 4.8E-10 | 6.7E-10 |
| Female Caucasians | | | | | | | |
| Cluster | 1 | 2 | 3 | 4 | 5 | 6 | 7 |
| B0 | 1.151 | 1.306 | 1.591 | 1.809 | 2.082 | 2.422 | 2.703 |
| B1 | -0.0127 | -0.01402 | -0.01846 | -0.02014 | -0.02105 | -0.02005 | -0.01681 |
| MeanX | 44.5 | 44.5 | 44.5 | 44.5 | 44.5 | 44.5 | 44.5 |
| B2 | 0.001199 | 0.001065 | 0.001112 | 0.001134 | 0.001079 | 0.0008929 | 0.0008952 |
| B3 | 0.00004054 | -0.0000239 | 0.0000831 | 0.00007474 | 0.00006216 | 0.00002339 | 0.00004406 |
| B4 | -0.00002038 | -0.00001444 | -0.00001818 | -0.00001861 | -0.00001538 | -0.00001134 | -0.00001648 |
| B5 | 2.351E-09 | 9.92E-09 | 1.955E-09 | 3.811E-09 | 5.484E-09 | 8.642E-09 | 3.48E-09 |
| B6 | 8.353E-10 | 4.694E-10 | 7.076E-10 | 7.102E-10 | 4.674E-10 | 2.625E-10 | 7.113E-10 |
| Male Asians | | | | | | | |
| Group | 1 | 2 | 3 | 4 | 5 | 6 | 7 |
| B0 | 1.482 | 1.717 | 1.945 | 2.163 | 2.365 | 2.638 | 3.009 |
| B1 | -0.02182 | -0.02545 | -0.02641 | -0.02549 | -0.02597 | -0.02492 | -0.02338 |
| MeanX | 37.61 | 37.61 | 37.61 | 37.61 | 37.61 | 37.61 | 37.61 |
| B2 | 0.0003261 | 0.0007227 | -0.00001075 | -0.0001564 | -0.0003498 | -0.0004978 | -0.000458 |
| B3 | 0.00001925 | 0.000024 | 0.00001789 | 0.00001272 | 0.00001237 | 0.000008992 | 0.00001318 |
| B4 | -4.698E-07 | -0.00002113 | -1.331E-07 | 4.836E-07 | 0.00001249 | 0.000001605 | 0.000001296 |
| B5 | -3.094E-09 | -7.626E-09 | 4.791E-09 | 1.226E-08 | 1.368E-08 | 1.659E-08 | 6.892E-09 |
| B6 | 1.519E-09 | 1.519E-09 | -6.122E-10 | -6.122E-10 | -1.273E-09 | -1.459E-09 | -1.212E-09 |
| Female Asians | | | | | | | |
| Group | 1 | 2 | 3 | 4 | 5 | 6 | 7 |
| B0 | 1.433 | 1.674 | 1.847 | 2.098 | 2.263 | 2.502 | 2.87 |
| B1 | -0.006877 | -0.01335 | -0.02078 | -0.02186 | -0.02304 | -0.0222 | -0.01746 |
| MeanX | 36.82 | 36.82 | 36.82 | 36.82 | 36.82 | 36.82 | 36.82 |
| B2 | -0.0003407 | -0.0002098 | -0.0000603 | -0.0001375 | -0.0001766 | -0.00005162 | -0.0002119 |
| B3 | -0.00004681 | -0.00003303 | 0.000006767 | 0.000008579 | 0.00001609 | 0.00001727 | 0.00007049 |
| B4 | 6.921E-07 | 1.766E-07 | -9.186E-08 | 6.834E-09 | 0.00000116 | -1.868E-07 | 4.975E-07 |
| B5 | 5.585E-08 | 4.467E-08 | 1.97E-09 | -3.01E-10 | -8.699E-09 | -1.285E-08 | -2.325E-09 |
| B6 | -6.996E-10 | -2.423E-10 | -6.996E-10 | -6.996E-10 | -1.273E-09 | -1.459E-09 | -5.06E-10 |

For male and female Caucasians, these were sixth order polynomials. For male and female Asians, these were either fifth or sixth order polynomials determined using extra sum-of-squares F-tests.

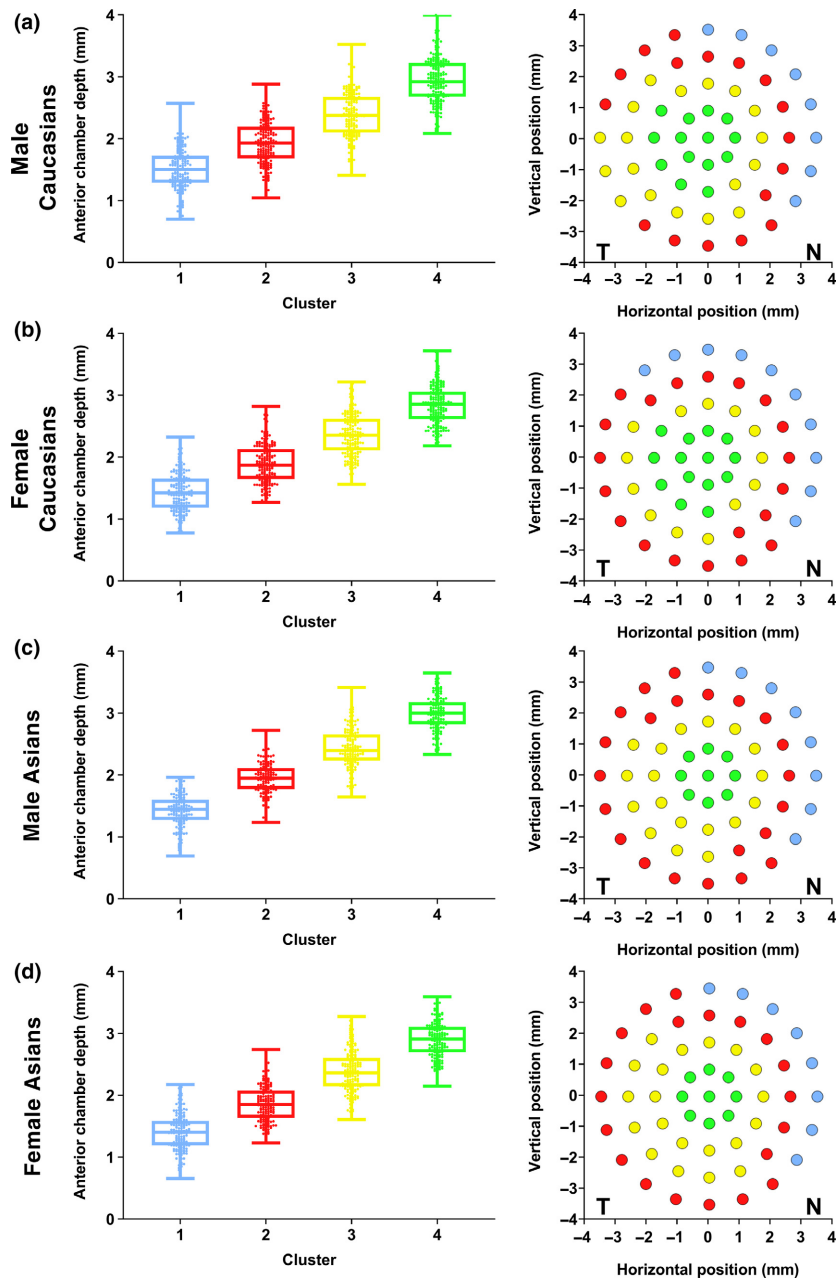


Figure 2. The distribution of age-corrected anterior chamber depth (mm) across the four cohorts in the present study (rows a-d). Left: box-and-whisker plots (median, interquartile range, full range) of the distribution of depth for each grouped cluster. Individual datum points represent the result of one subject at one location within the chamber width. Each colour on the left panel corresponds to the same coloured cluster on the right hand side maps. Right: theme maps representing groups of test locations with statistically identical distributions of anterior chamber depth found using hierarchical cluster analysis. The axes indicate the physical position of the test location (N, nasal; T, temporal). Separability analyses are shown in Table 3 and distribution characteristics are shown in Table 4.

were primarily in the width of the 95% limits of agreement and standard deviation, but again, this was relatively small. These are reported and compared in Supplementary Figures S1-S4 and the different polynomial fits are shown in Supplementary Tables S1-S4.

3.4. Effect of spherical equivalent refractive error

There was a statistically significant relationship between spherical equivalent refractive error and anterior chamber depth at nearly all test locations ($p < 0.05$ for all); only the

Table 3. Separability (d-prime) calculations for each final cluster group for each cohort

| | | Cluster 1 | Cluster 2 | Cluster 3 | Cluster 4 |
|-------------------|-------------|-------------|-------------|-------------|-------------|
| Male Caucasians | | | | | |
| Cluster 1 | 1.51 (0.35) | 1.51 (0.35) | 1.92 (0.40) | 2.39 (0.42) | 2.93 (0.40) |
| Cluster 2 | 1.92 (0.40) | 1.10 | | | |
| Cluster 3 | 2.39 (0.42) | 2.27 | 1.14 | | |
| Cluster 4 | 2.93 (0.40) | 3.78 | 2.53 | 1.32 | |
| Female Caucasians | | | | | |
| Cluster 1 | 1.45 (0.32) | 1.45 (0.32) | 1.88 (0.37) | 2.37 (0.34) | 2.84 (0.36) |
| Cluster 2 | 1.88 (0.37) | 1.24 | | | |
| Cluster 3 | 2.37 (0.34) | 2.8 | 1.39 | | |
| Cluster 4 | 2.84 (0.36) | 4.09 | 2.65 | 1.35 | |
| Male Asians | | | | | |
| Cluster 1 | 1.43 (0.26) | 1.43 (0.26) | 1.92 (0.33) | 2.36 (0.43) | 3.00 (0.28) |
| Cluster 2 | 1.92 (0.33) | 1.65 | | | |
| Cluster 3 | 2.36 (0.43) | 2.58 | 1.12 | | |
| Cluster 4 | 3.00 (0.28) | 5.78 | 3.5 | 1.76 | |
| Female Asians | | | | | |
| Cluster 1 | 1.41 (0.36) | 1.41 (0.36) | 1.88 (0.39) | 2.40 (0.41) | 2.90 (0.31) |
| Cluster 2 | 1.88 (0.39) | 1.26 | | | |
| Cluster 3 | 2.40 (0.41) | 2.57 | 1.28 | | |
| Cluster 4 | 2.90 (0.31) | 4.44 | 2.87 | 1.38 | |

Each cluster represents a statistically separable group of test locations (as per Figure 2) with a d-prime of >1 from other clusters. Mean and standard deviation (in brackets) for each cluster is shown.

superior test locations for both Asian cohorts did not show a significant relationship. The fits of the regression analyses were generally poor for the male Caucasian ($R^2 = 0.12$ – 0.27) and both Asian cohorts ($R^2 = 0.01$ – 0.15), but was better for the female Caucasian group ($R^2 = 0.17$ – 0.30). There was no significant difference in slope across all test locations ($p > 0.99$ for all cohorts), indicating that the relationship with refractive error and chamber depth was uniform across the chamber width. The average slopes were: -0.097 , -0.1027 , -0.048 and -0.048 for male Caucasian, female Caucasian, male Asian and female Asian groups, respectively.

Following the age-correction process described above, all regression slopes describing the relationship between refractive error and chamber depth were flatter, though this change was significantly only for the female Caucasian group. Again, F -test showed no significant difference across location within each group ($p > 0.99$), with the final pooled slopes as follows: -0.067 , -0.060 , -0.030 and -0.025 for male Caucasian, female Caucasian, male Asian and female Asian groups, respectively. The R^2 values were notably poorer across all groups ($p < 0.0001$), ranging from 0.001 to 0.23. Results at three representative test locations are shown in Figure 4.

To examine the effect of refractive error further, we used the regression analysis results derived above to correct subjects to a 0 dioptre spherical equivalent and re-performed cluster analysis; following this, age-correction was performed to identify age-corrected clusters, and then finally Bland-Altman comparison with the ground truth as described above. Results for the female Caucasian group are shown in Figure 5, as the relationship between refractive error and depth was strongest here. There were almost no differences in cluster group assignment for age-related clusters and age-corrected clusters in comparison to models that did not factor in refractive error correction. Bland-Altman analysis showed a slightly smaller mean bias (difference 1.3%) in comparison to the above model without incorporating refractive correction. The same analysis performed on male Caucasians, male Asians and female Asians (Supplementary Figures S5–S7) showed a greater magnitude of overall bias in comparison to the non-refractive models. The modified age-correction factors following initial refractive correction are shown in Supplementary Table S5. The resultant age-corrected (35-year-old equivalent) mean, standard deviation and calculated distribution limits for each cohort are shown in Supplementary Table S6, with only slight differences with the non-refractive-corrected results shown in Table 4.

Table 4. Mean, standard deviation (SD) and calculated 95% distribution limits of anterior chamber depths across each age-corrected cluster (leftmost column) for each gender and ethnicity cohort

| Cluster | Male Caucasians | | Female Caucasians | | Male Asians | | Female Asians | |
|---------|-----------------|-------------------------|-------------------|-------------------------|-------------|-------------------------|---------------|-------------------------|
| | Mean (SD) | 95% distribution limits | Mean (SD) | 95% distribution limits | Mean (SD) | 95% distribution limits | Mean (SD) | 95% distribution limits |
| 1 | 1.52 (0.36) | 0.81, 2.23 | 1.45 (0.32) | 0.82, 2.08 | 1.52 (0.26) | 1.01, 2.04 | 1.44 (0.30) | 0.86, 2.02 |
| 2 | 1.93 (0.39) | 1.16, 2.70 | 1.88 (0.37) | 1.16, 2.60 | 2.01 (0.32) | 1.39, 2.64 | 1.87 (0.34) | 1.21, 2.53 |
| 3 | 2.39 (0.42) | 1.57, 3.21 | 2.33 (0.38) | 1.57, 3.08 | 2.50 (0.35) | 1.81, 3.19 | 2.32 (0.40) | 1.53, 3.11 |
| 4 | 2.93 (0.40) | 2.15, 3.71 | 2.84 (0.36) | 2.14, 3.54 | 3.06 (0.29) | 2.49, 3.62 | 2.90 (0.30) | 2.31, 3.50 |

3.5. Assessing literature-reported anterior chamber depth cut-off values for angle closure

Table 5 shows the percentile values within our four age-corrected normal cohorts using the results from four studies in the literature reporting on Scheimpflug imaging in angle closure disease. We compared their central anterior chamber depth results with the equivalent location in our results (i.e. cluster group 1). The percentile of the cut-off values reported by each study differed across each of the normative cohorts reported in the present study; specifically, the typical criterion of $p < 0.05$ level of significance was only met four out of 16 times the cut-offs were compared with our normative cohort.

Given that only central anterior chamber depth cut-offs have been reported in the above studies, we also performed a comparison between male Caucasian and female Asian cohorts – the pair with the greatest differences on multiple comparisons across the chamber width. Three representative locations were selected for examination (Figure 6). The clinical implication of using different normative data for comparisons is apparent: aside from differences at the central chamber depth position shown in Table 5, there can be large errors in interpretation where there are discordances in underlying distribution characteristics (e.g. locations 2 and 3 in Figure 6).

4. Discussion

In the present study, we leveraged the application of clustering techniques to identify age-, gender-, refractive- and ethnicity-related changes in anterior chamber depth across the central chamber width. In doing so, we were able to identify asymmetric age-corrected clusters of iso-depth across the chamber width to form the basis of normative distributions for comparisons to highlight areas of anomaly. This clustering approach has previously been applied in biological variables (both anatomical (retinal³⁹ and corneal²⁶) and functional (perimetric^{23,24}) data) and for classification within specific diagnoses for potential subgroup phenotyping.^{40,41} The advantage of this clustering approach is that no assumptions regarding spatial arrangement are

made *a priori*, and hence the specific clusters are identified on the basis of underlying distribution alone. In doing so, we have provided robust estimations of age-related changes and iso-depth patterns. Given differences in age-related changes across the chamber width, failing to account for age- and gender-related changes in depth has implications for performing normative comparisons.

4.1. Age- and gender-related changes in the anterior chamber

Anterior chamber parameters have been shown to shallow with age, and previous studies have largely focussed on central anterior chamber depth. Although studies have commonly described these changes in a linear fashion,^{18,42} Foster *et al*¹⁵ demonstrated that a cubic function best described the age-related change, with a maximal rate of change occurring between 30 and 60 years. Wojciechowski *et al*¹⁹ also suggested a nonlinear change in anterior chamber depth over time. The results of the present study provide further support for nonlinear changes over time, though we present models of different complexity that have similar overall magnitudes of bias with respect to age-correction. One reason for the potential complexity of the model is the change occurring in both the lens and the cornea, which play a role in determining anterior chamber depth. We have recently demonstrated that corneal curvature and thickness also change in a nonlinear fashion, and additionally with ring-like patterns, with age.²⁵ The ring-like patterns of corneal change may contribute to the clusters identified in the present study. Lens capsule thickness has also been shown to have different thicknesses and rates of change over different areas, and again could account for regional clusters of age-related change.⁴³ The body of the lens itself thickens with age, and has interestingly been shown to also follow a nonlinear trend over time.⁴⁴ Garcia-Domene *et al*⁴⁴ specifically noted that polynomial functions may provide better fits of their lens data similar to the work of Dalziel and Egan,⁴⁵ but have offered that a logarithmic fit is simpler overall. Our findings of age-related anterior chamber depth change may also be an epiphenomenon due to increased lenticular-related chamber crowding with age.

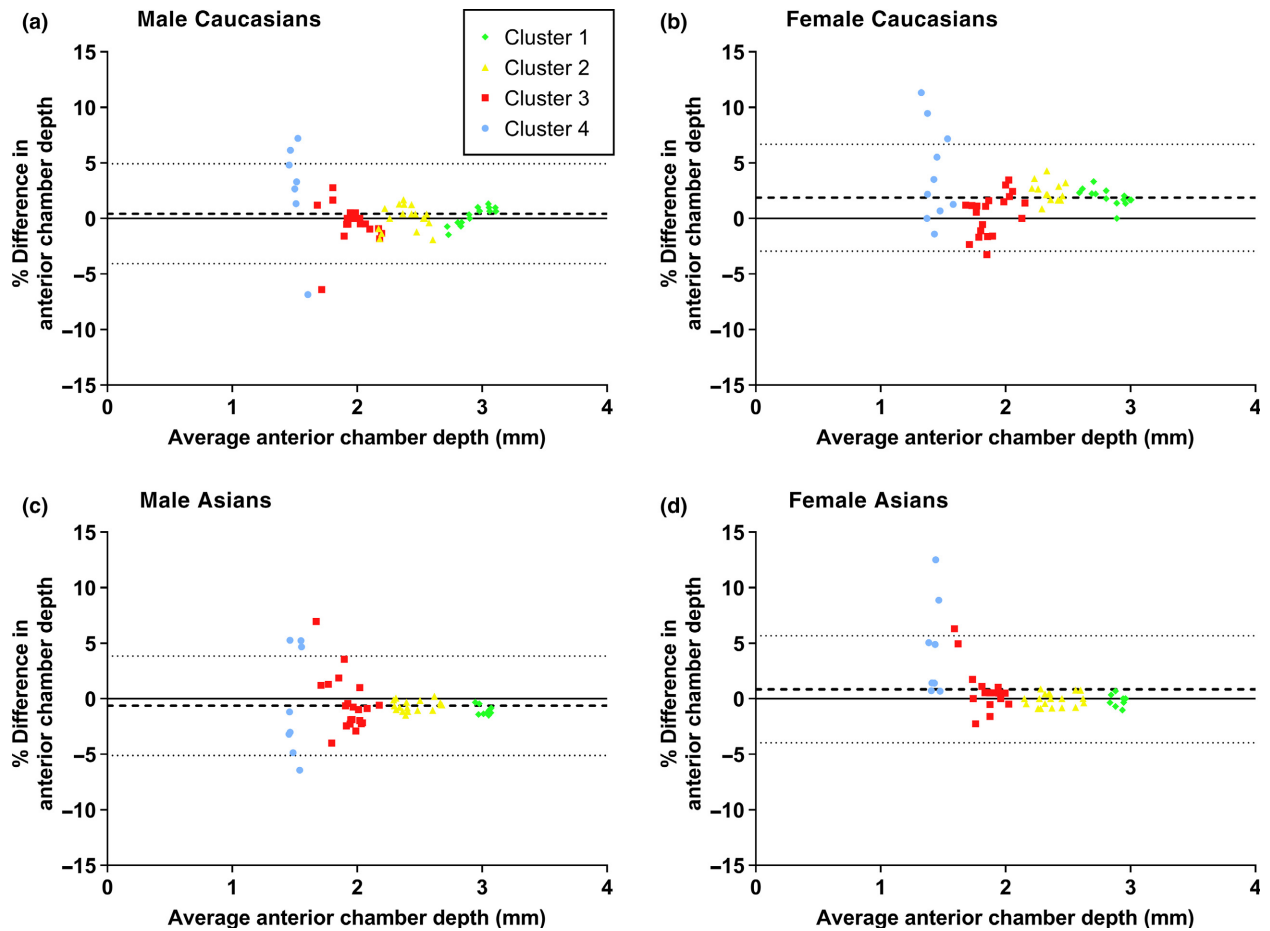


Figure 3. Bland-Altman analysis comparing the age-corrected anterior chamber depth (excluding 30–40 year old subjects) with the ground truth group of 30–40 year old subjects across the four cohorts in the present study. To compare locations, genders and ethnicities fairly, without prior assumptions regarding specific depths, percentage differences are reported. Individual datum points represent one test location within the chamber width. Each colour corresponds to the same coloured cluster as in Figure 2. The black dashed horizontal line indicates the mean bias, and the black dotted lines indicate the 95% limits of agreement for the aggregate data for each cohort.

Our results were concordant with studies demonstrating shallower anterior chamber depth measurements in females compared to males, independent of instrument or technique.^{15,42,46,47} This is hypothesised to be due to smaller anthropomorphic measurements.^{17,20,48} Although there was a tendency for Asian eyes to have shallower depths, we were unable to find a statistically significant difference in the distribution characteristics of age-corrected chamber depths between Caucasian and Asian individuals of the same gender. Given estimates of the standard deviation of central anterior chamber depth measurements reported in the literature (~0.07 mm),⁴⁹ our sample size of > 160 was more than sufficient for identifying these differences given at least 80% power.

4.2. Effect of spherical equivalent refractive error

As expected, increased hyperopic spherical equivalent refractive error was associated with a shallower anterior

chamber depth, as per previous studies.^{17,18,28} Interestingly, the effect appeared greatest in the female Caucasian group within the present study, which suggests an interaction with gender and ethnicity, the former of which was also suggested by Foster *et al.*⁵⁰ However, the overall coefficients of determination were low, suggesting that refractive error only played a small role in accounting for chamber depth in the present cohort. Addition of the refractive-correction mostly affected the peripheral test locations, and this may be due to inherent limitations of imaging the peripheral chamber depth, as there were fewer reliable test locations overall. There was the introduction of a greater magnitude of bias in the comparisons with the ground truth for groups aside from female Caucasians, suggesting that refractive-correction of these models may be unnecessary. Further study is required with a greater diversity of refractive errors within each age group to examine this.

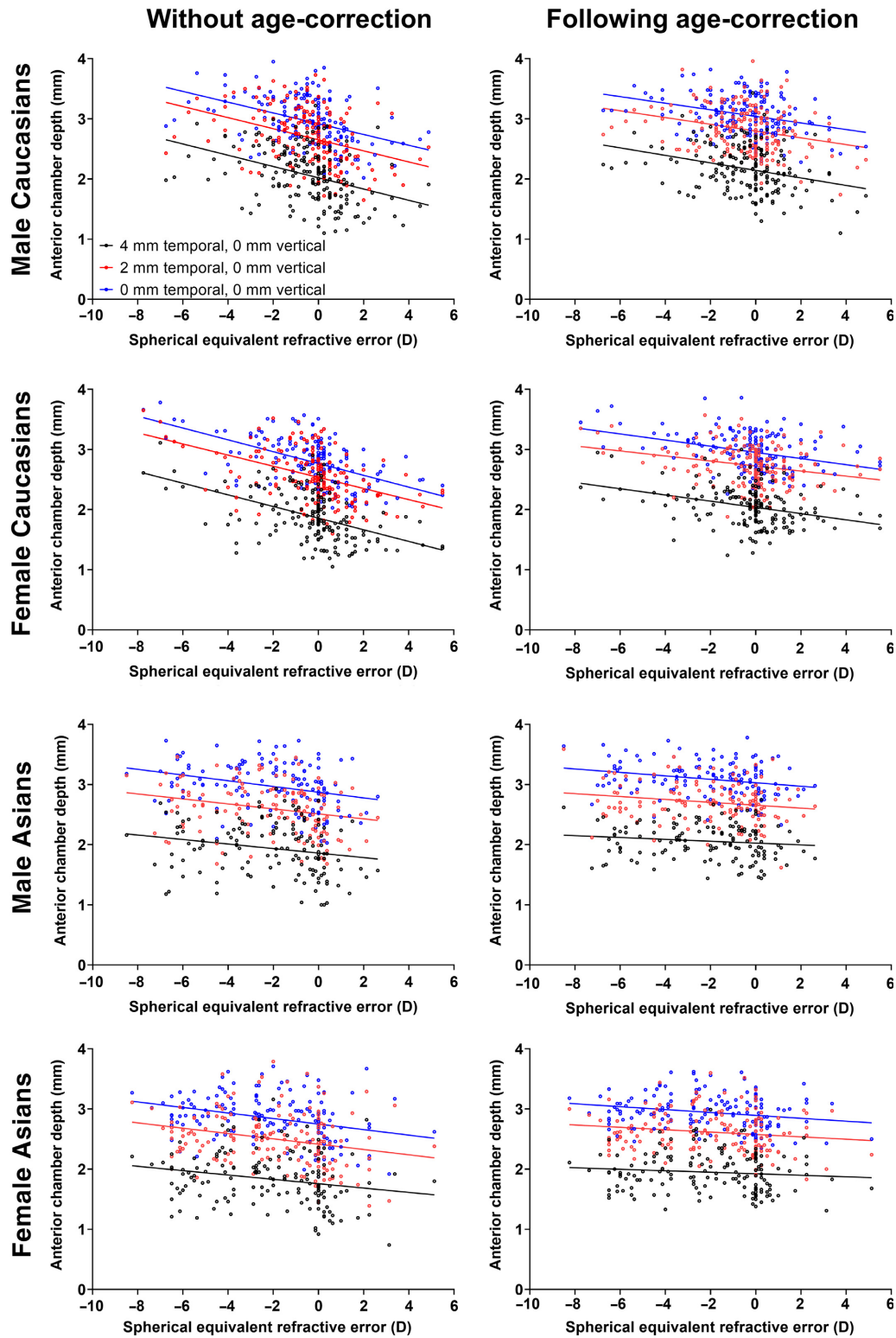


Figure 4. Linear regression analysis of anterior chamber depth (mm) as a function of spherical equivalent refractive error (dioptres) at four representative test locations (black: 4 mm temporal; red, 2 mm temporal; blue, 0 mm temporal along the horizontal meridian) for each cohort. Left: analysis performed prior to applying age-correction factors to the cohort. Right: analysis performed following the application of age-correction factors described in Figure 1 to the cohort. As the regression slopes were statistically identical, they are described in the text.

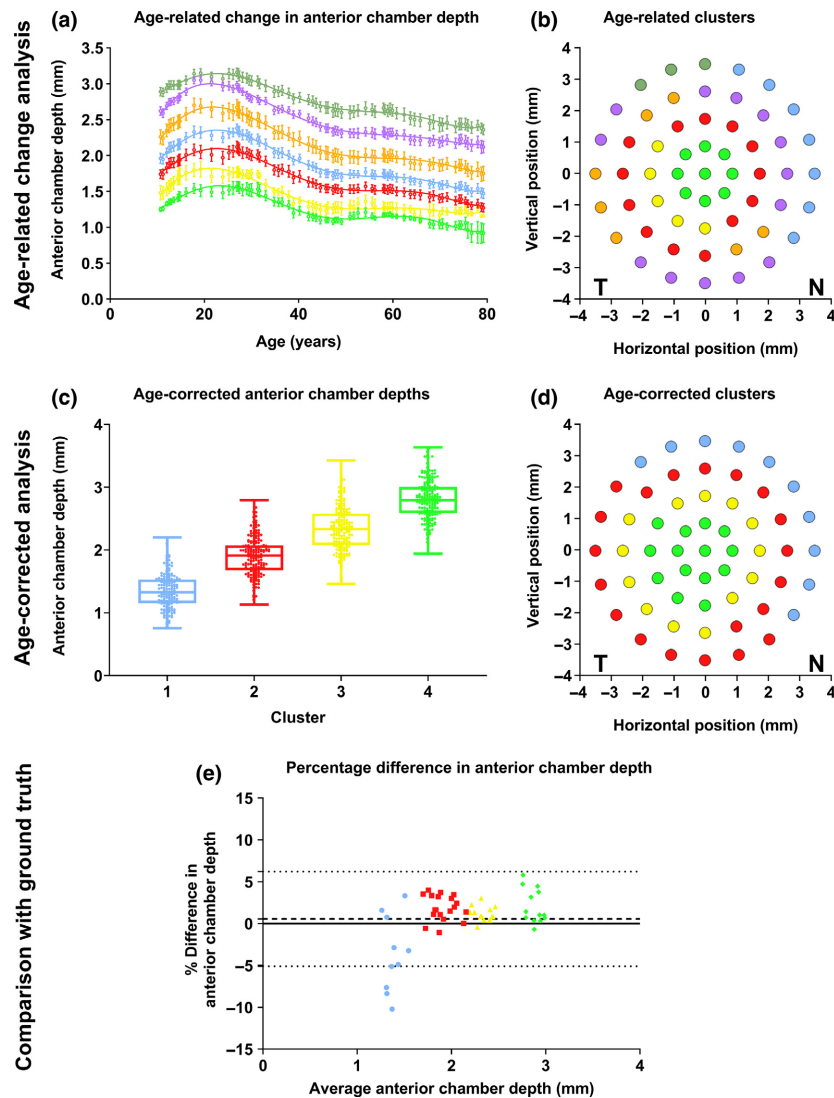


Figure 5. Analysis of age-related changes (top), distributions of age-corrected chamber depth (middle) and Bland-Altman comparison of age-corrected depths against the ground truth 30 to 40-year-old cohort (bottom) for the refraction-corrected female Caucasian group. Top: nonlinear regression analysis of chamber depth (mm) as a function of age (year) using the sliding window method (a) and cluster map of test locations with statistically identical age-related changes in depth (b), as per Figure 1. Middle: box-and-whisker plots (median, interquartile range, full range) of age-corrected chamber depth (mm) (c) for each cluster of test locations with statistically identical distribution characteristics (d), as per Figure 2. E: Bland-Altman comparisons plotted for each of the age-corrected four clusters identified in D, as per Figure 4.

4.3. Applications in the diagnosis and screening of angle closure spectrum disease

In angle closure spectrum disease, indices suggested for screening obtained using anterior segment imaging have included anterior chamber width, volume and depth.³⁸ The physiological basis behind the shallowing or narrowing of these parameters in angle closure spectrum disease has been discussed previously.⁵¹

The reported efficacy of quantitative anterior chamber metrics has been variable. Methodological and demographic differences, in part, have accounted for some

differences, but there has been little in terms of reconciling discordances in cut-off values reported in previous work. Overestimation of diagnostic accuracy has also been suggested due to the case-control design of some studies. Our results suggest the role of both age and gender, and a dynamic course of chamber depth over time.

Two specific metrics that have been frequently reported and compared in the literature are central anterior chamber depth and limbal (peripheral) anterior chamber depth.^{33,37,52} However, it is further possible that some of the pathological-related events occur between the central anterior chamber region and peripheral limbal chamber

Table 5. Comparison of predicted equivalent ages using the models in the present study for a given central anterior chamber depth cut-off value for angle closure disease when using reference central anterior chamber depth cut-off values and mean age of subjects for four different studies

| Study | Central anterior chamber depth cut-off value (mm) | Mean age of subjects with angle closure disease within study (years) | Equivalent age-corrected chamber depth (mm) ¹ | | | | Percentile within age-corrected normal distribution ² | | | |
|-----------------------|---|--|--|------------------|------------|--------------|--|------------------|------------|--------------|
| | | | Male Caucasian | Female Caucasian | Male Asian | Female Asian | Male Caucasian | Female Caucasian | Male Asian | Female Asian |
| Kurita et al (2009) | 2.58 | 58.40 | 2.78 | 2.62 | 2.60 | 2.55 | 27.1 | 44.5 | 47.7 | 54.4 |
| George et al (2003) | 2.53 | 57.45 | 2.79 | 2.63 | 2.61 | 2.56 | 22.0 | 38.9 | 40.7 | 45.7 |
| Pakravan et al (2012) | 2.1 | 59.00 | 2.78 | 2.62 | 2.61 | 2.54 | 2.1 | 5.0 | 6.1 | 6.7 |
| Rossi et al (2012) | 1.93 | 66.10 | 2.70 | 2.56 | 2.62 | 2.41 | 1.1 | 2.4 | 1.5 | 5.2 |

¹Equivalent normal central anterior chamber depth was taken by inputting the mean age of participants in the study into the age-related change models in the present study.

²These equivalent chamber depths were then used to calculate the percentile position within the normal distribution for each cut-off value proposed by each of the four studies.

depth. We now provide normative data and distributions for paracentral depths, which may provide an additional dimension for characterising and diagnosing angle closure spectrum disease. Understanding the changes to anterior segment parameters within an eye occurring over time would be informative in determining which changes are age-related normal processes versus pathological events.⁵³ Patterns of age-related changes can also be applied to stratify the risk of subsequent development of angle closure spectrum disease.

In terms of clinical interpretation, although the distribution characteristics of corresponding age-corrected clusters showed almost no difference between groups, the class assignment, and whether a particular test point lies within one cluster or its adjacent cluster, may affect validity in normative comparisons, as illustrated in Figure 6.

4.4. Limitations

A limitation of the study was regarding the sample of patients within the upper age ranges (>65 years). Although most data points were available for these groups, there were often data gaps due to lid anomalies, most notably for the Asian male and female cohorts. Our study used a sample of convenience and so was not fully representative of a truly random sample from the population; we tried to mitigate this by using a diverse age range and large sample size for each cohort. We also did not have axial length measurements for the patients. For the purposes of angle closure disease, recent commentary has highlighted the importance of anterior segment biometry in lieu of whole eye biometry: it is more important to consider anterior chamber parameters, which may be discordant to axial length.⁵⁴ Other biometric factors such as iris thickness are not readily measured using the Scheimpflug technique, which could be further investigated in future work.

Since cataract surgery is a common procedure in individuals 60–70 years old,⁵⁵ the value of measuring anterior chamber depth using techniques such as Scheimpflug imaging is also expected to diminish over time with a deepening of the chamber following the procedure. Understanding the role of lenticular changes on the chamber would necessitate a specifically larger cohort for this purpose, but could provide further insight into the pathophysiology of lens-related angle closure.

Our study utilised self-reported ethnicity in an Australian clinic; these results may be subtly different to other health care settings, and a degree of self-selection may exist. The homogeneity of the ethnic groups could have also differed, contributing to the differences in quality of polynomial fits. Ethnicity differences in different settings may potentially account for different mechanisms of angle closure across ethnicities.^{56–58} Future studies could adopt this methodology to determine if there exist systematic differences in patterns of chamber depth in different contexts.

Finally, we used a combination clustering and separability analyses that we have leveraged in previous work.^{24,26,27} Other clustering methods, such as K-means, may present slightly different results. Our previous work suggests that the K-means and hierarchical agglomerative clustering methods generally produce similar results, so long as the underlying data set is suitably robust in its distribution characteristics.²⁴ We attempted to mitigate the possibility of differences arising due to sampling by using a sliding window analysis, but as alluded to above, the ideal data set would include many more individual subjects sampled from the general population.

5. Conclusions

There are clusters of age-related changes in anterior chamber depth across the chamber width that are gender- and

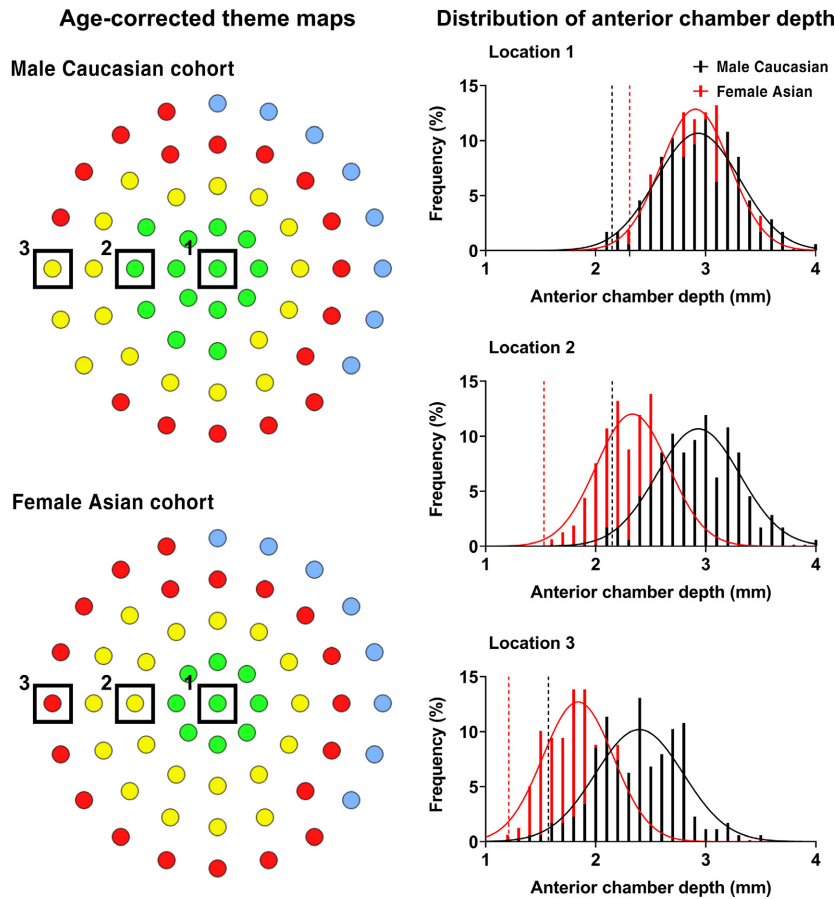


Figure 6. Comparison of distribution limits between male Caucasian and female Asian cohorts at three representative locations. Left: age-corrected anterior chamber depth theme maps from Figure 2 are shown with the three black inset boxes indicating the three tested locations. Note that location 1 belongs to group 4 in both cohorts; however, locations 2 and 3 belong to different groups. Right: distribution of anterior chamber depth at each location for both cohorts (black, male Caucasians; red, female Asians). Gaussian distributions have been fitted to the frequency histograms. The vertical dashed lines indicate the 2.5th percentile (lower of the 95% distribution limit) for the respective cohorts.

ethnicity-specific. These clusters need to be accounted for when analysing potential pathological changes to the anterior chamber such as in angle closure disease. Our results temper the ability for quantitative data from Scheimpflug imaging to detect angle closure in isolation given the wide distribution limits.

Acknowledgements

Guide Dogs NSW/ACT provides funding for clinical services delivered at the Centre for Eye Health, where the patient data was collected. JP, JT, BZ and MK all receive salary support from Guide Dogs NSW/ACT. JLL was supported by a Summer Vacation Research Scholarship funded by Guide Dogs NSW/ACT. The funding body played no role in the conception or conduct of the study. JP, JT, BZ and MK are named inventors on

a provisional patent involving the use of cluster analysis to the anterior segment for diagnosis and prognostication: ‘A clustering method to analyse clinical topographic data from the anterior eye for disease management, change and/or progression’ Australian Provisional Patent Application No. 2019902873, filed August 12, 2019.

Conflict of interest

JP, JT, BZ and MK are named inventors on a provisional patent involving the use of cluster analysis to the anterior segment for diagnosis and prognostication: “A clustering method to analyse clinical topographic data from the anterior eye for disease management, change and/or progression” Australian Provisional Patent Application No. 2019902873, filed August 12, 2019.

References

1. Tham YC, Li X, Wong TY *et al.* Global prevalence of glaucoma and projections of glaucoma burden through 2040: a systematic review and meta-analysis. *Ophthalmology* 2014; 121: 2081–2090.
2. Quigley HA & Broman AT. The number of people with glaucoma worldwide in 2010 and 2020. *Br J Ophthalmol* 2006; 90: 262–267.
3. Cook C & Foster P. Epidemiology of glaucoma: what's new? *Can J Ophthalmol* 2012; 47: 223–226.
4. Chan EW, Li X, Tham YC *et al.* Glaucoma in Asia: regional prevalence variations and future projections. *Br J Ophthalmol* 2016; 100: 78–85.
5. Vajaranant TS, Nayak S, Wilensky JT & Joslin CE. Gender and glaucoma: what we know and what we need to know. *Curr Opin Ophthalmol* 2010; 21: 91–99.
6. Smith SD, Singh K, Lin SC *et al.* Evaluation of the anterior chamber angle in glaucoma: a report by the american academy of ophthalmology. *Ophthalmology* 2013; 120: 1985–1997.
7. Phu J, Wang H, Khuu SK *et al.* Anterior chamber angle evaluation using gonioscopy: consistency and agreement between optometrists and ophthalmologists. *Optom Vis Sci* 2019; 96: 751–760.
8. Friedman DS & He M. Anterior chamber angle assessment techniques. *Surv Ophthalmol* 2008; 53: 250–273.
9. Phu J, Wang H, Khou V *et al.* Remote grading of the anterior chamber angle using gonioscopic photographs and optical coherence tomography: implications for telemedicine or virtual clinics. *Transl Vis Sci Technol* 2019; 8: 16.
10. Rabsilber TM, Khoramnia R & Auffarth GU. Anterior chamber measurements using Pentacam rotating Scheimpflug camera. *J Cataract Refract Surg* 2006; 32: 456–459.
11. Grewal DS, Brar GS, Jain R & Grewal SP. Comparison of Scheimpflug imaging and spectral domain anterior segment optical coherence tomography for detection of narrow anterior chamber angles. *Eye (Lond)* 2011; 25: 603–611.
12. Pakravan M, Sharifpour F, Yazdani S *et al.* Scheimpflug imaging criteria for identifying eyes at high risk of acute angle closure. *J Ophthalmic Vis Res* 2012; 7: 111–117.
13. Winegarner A, Miki A, Kumoi M *et al.* Anterior segment Scheimpflug imaging for detecting primary angle closure disease. *Graefes Arch Clin Exp Ophthalmol* 2019; 257: 161–167.
14. Kurita N, Mayama C, Tomidokoro A *et al.* Potential of the pentacam in screening for primary angle closure and primary angle closure suspect. *J Glaucoma* 2009; 18: 506–512.
15. Foster PJ, Alsbirk PH, Baasanhu J *et al.* Anterior chamber depth in Mongolians: variation with age, sex, and method of measurement. *Am J Ophthalmol* 1997; 124: 53–60.
16. Leung CK, Palmiero PM, Weinreb RN *et al.* Comparisons of anterior segment biometry between Chinese and Caucasians using anterior segment optical coherence tomography. *Br J Ophthalmol* 2010; 94: 1184–1189.
17. Schuster AK, Pfeiffer N, Nickels S *et al.* Distribution of anterior chamber angle width and correlation with age, refraction, and anterior chamber depth—the Gutenberg health study. *Invest Ophthalmol Vis Sci* 2016; 57: 3740–3746.
18. Shajari M, Herrmann K, Bühren J *et al.* Anterior chamber angle, volume, and depth in a normative cohort—a retrospective cross-sectional study. *Curr Eye Res* 2019; 44: 632–637.
19. Wojciechowski R, Congdon N, Anninger W & Teo Broman A. Age, gender, biometry, refractive error, and the anterior chamber angle among Alaskan Eskimos. *Ophthalmology* 2003; 110: 365–375.
20. Xu L, Li JJ, Xia CR *et al.* Anterior chamber depth correlated with anthropomorphic measurements: the Beijing Eye Study. *Eye (Lond)* 2009; 23: 632–4.
21. Zhang X, Liu Y, Wang W *et al.* Why does acute primary angle closure happen? Potential risk factors for acute primary angle closure. *Surv Ophthalmol* 2017; 62: 635–647.
22. Foster PJ. The epidemiology of primary angle closure and associated glaucomatous optic neuropathy. *Semin Ophthalmol* 2002; 17: 50–58.
23. Phu J, Khuu SK, Bui BV & Kalloniatis M. Application of Pattern Recognition Analysis to Optimize Hemifield Asymmetry Patterns for Early Detection of Glaucoma. *Transl Vis Sci Technol* 2018; 7: 3.
24. Phu J, Khuu SK, Nivison-Smith L *et al.* Pattern recognition analysis reveals unique contrast sensitivity isocontours using static perimetry thresholds across the visual field. *Invest Ophthalmol Vis Sci* 2017; 58: 4863–76.
25. Tong J, Phu J, Kalloniatis M & Zangerl B. Modeling changes in corneal parameters with age: implications for corneal disease detection. *Am J Ophthalmol* 2020; 209: 117–31.
26. Tong J, Phu J, Khuu SK *et al.* Development of a spatial model of age-related change in the macular ganglion cell layer to predict function from structural changes. *Am J Ophthalmol* 2019; 208: 166–177.
27. Yoshioka N, Zangerl B, Phu J *et al.* Consistency of structure-function correlation between spatially scaled visual field stimuli and In Vivo OCT Ganglion cell counts. *Invest Ophthalmol Vis Sci* 2018; 59: 1693–1703.
28. Orucoglu F, Akman M & Onal S. Analysis of age, refractive error and gender related changes of the cornea and the anterior segment of the eye with Scheimpflug imaging. *Cont Lens Anterior Eye* 2015; 38: 345–350.
29. Li Y & Bao FJ. Interocular symmetry analysis of bilateral eyes. *J Med Eng Technol* 2014; 38: 179–187.
30. Almeida DL, Soares FA & Carvalho JL. A sliding window approach to detrended fluctuation analysis of heart rate variability. *Conf Proc IEEE Eng Med Biol Soc* 2013; 2013: 3278–3281.
31. Varshavsky R, Horn D & Linial M. Global considerations in hierarchical clustering reveal meaningful patterns in data. *PLoS One* 2008; 3: e2247.
32. Yap BW & Sim CH. Comparisons of various types of normality tests. *J Stat Comput Sim* 2011; 81: 2141–2155.

33. Dabasia PL, Edgar DF, Murdoch IE & Lawrenson JG. Non-contact screening methods for the detection of narrow anterior chamber angles. *Invest Ophthalmol Vis Sci* 2015; 56: 3929–3935.
34. Rossi GC, Scudeller L, Delfino A *et al.* Pentacam sensitivity and specificity in detecting occludable angles. *Eur J Ophthalmol* 2012; 22: 701–708.
35. Alonso RS, Ambrosio Junior R, Paranhos Junior A *et al.* Glaucoma anterior chamber morphometry based on optical Scheimpflug images. *Arq Bras Oftalmol* 2010; 73: 497–500.
36. Hong S, Yi JH, Kang SY *et al.* Detection of occludable angles with the Pentacam and the anterior segment optical coherence tomography. *Yonsei Med J* 2009; 50: 525–8.
37. Zhang Y, Li SZ, Li L *et al.* The Handan Eye Study: comparison of screening methods for primary angle closure suspects in a rural Chinese population. *Ophthalmic Epidemiol* 2014; 21: 268–275.
38. Lavanya R, Foster PJ, Sakata LM *et al.* Screening for narrow angles in the singapore population: evaluation of new non-contact screening methods. *Ophthalmology* 2008; 115: 1720–1727, 7 e1–2
39. Yoshioka N, Zangerl B, Nivison-Smith L *et al.* Pattern recognition analysis of age-related retinal ganglion cell signatures in the human eye. *Invest Ophthalmol Vis Sci* 2017; 58: 3086–3099.
40. Bae HW, Ji Y, Lee HS *et al.* A hierarchical cluster analysis of normal-tension glaucoma using spectral-domain optical coherence tomography parameters. *J Glaucoma* 2015; 24: 328–333.
41. Bae HW, Rho S, Lee HS *et al.* Hierarchical cluster analysis of progression patterns in open-angle glaucoma patients with medical treatment. *Invest Ophthalmol Vis Sci* 2014; 55: 3231–3236.
42. He M, Huang W, Zheng Y *et al.* Anterior chamber depth in elderly Chinese: the Liwan eye study. *Ophthalmology* 2008; 115: 1286–1290, 90 e1–2.
43. Barraquer RI, Michael R, Abreu R *et al.* Human lens capsule thickness as a function of age and location along the sagittal lens perimeter. *Invest Ophthalmol Vis Sci* 2006; 47: 2053–2060.
44. Garcia-Domene MC, Diez-Ajenjo MA, Gracia V *et al.* A simple description of age-related changes in crystalline lens thickness. *Eur J Ophthalmol* 2011; 21: 597–603.
45. Dalziel CC & Egan DJ. Crystalline lens thickness changes as observed by pachometry. *Am J Optom Physiol Opt* 1982; 59: 442–447.
46. Hashemi H, Khabazkhoob M, Miraftab M *et al.* The distribution of axial length, anterior chamber depth, lens thickness, and vitreous chamber depth in an adult population of Shahrud, Iran. *BMC Ophthalmol* 2012; 12: 50.
47. Xu L, Cao WF, Wang YX *et al.* Anterior chamber depth and chamber angle and their associations with ocular and general parameters: the Beijing Eye Study. *Am J Ophthalmol* 2008; 145: 929–936.
48. Jonas JB, Nangia V, Gupta R *et al.* Anterior chamber depth and its associations with ocular and general parameters in adults. *Clin Exp Ophthalmol* 2012; 40: 550–556.
49. Lackner B, Schmidinger G & Skorpik C. Validity and repeatability of anterior chamber depth measurements with Pentacam and Orbscan. *Optom Vis Sci* 2005; 82: 858–861.
50. Foster PJ, Broadway DC, Hayat S *et al.* Refractive error, axial length and anterior chamber depth of the eye in British adults: the EPIC-Norfolk Eye Study. *Br J Ophthalmol* 2010; 94: 827–830.
51. Sun X, Dai Y, Chen Y *et al.* Primary angle closure glaucoma: What we know and what we don't know. *Prog Retin Eye Res* 2017; 57: 26–45.
52. Nolan WP, Aung T, Machin D *et al.* Detection of narrow angles and established angle closure in Chinese residents of Singapore: potential screening tests. *Am J Ophthalmol* 2006; 141: 896–901.
53. Chen YY, Chen YY, Sheu SJ & Chou P. The biometric study in different stages of primary angle-closure glaucoma. *Eye (Lond)* 2013; 27: 1070–1076.
54. Yong KL, Gong T, Nongpiur ME *et al.* Myopia in asian subjects with primary angle closure: implications for glaucoma trends in East Asia. *Ophthalmology* 2014; 121: 1566–1571.
55. Lundstrom M, Goh PP, Henry Y *et al.* The changing pattern of cataract surgery indications: a 5-year study of 2 cataract surgery databases. *Ophthalmology* 2015; 122: 31–38.
56. Wang YE, Li Y, Wang D *et al.* Comparison of factors associated with occludable angle between american Caucasians and ethnic Chinese. *Invest Ophthalmol Vis Sci* 2013; 54: 7717–7723.
57. He M, Foster PJ, Johnson GJ & Khaw PT. Angle-closure glaucoma in East Asian and European people. Different diseases? *Eye (Lond)* 2006; 20: 3–12.
58. Ho H, Ozaki M, Mizoguchi T *et al.* Angle-closure glaucoma in Asians: comparison of biometric and anterior segment parameters between Japanese and Chinese subjects. *Graefes Arch Clin Exp Ophthalmol* 2015; 253: 601–608.

Supporting Information

Additional Supporting Information may be found in the online version of this article:

Figure S1. Bland-Altman analysis comparing the age-corrected anterior chamber depth with the ground truth group for male Caucasians for each of the regression analyses (sixth-, fifth-, fourth-, third- and second-order polynomial and linear).

Figure S2. Bland-Altman analysis comparing the age-corrected anterior chamber depth with the ground truth group for female Caucasians for each of the regression analyses (sixth-, fifth-, fourth-, third- and second-order polynomial and linear), depicted as per Supplementary Figure 1.

Figure S3. Bland-Altman analysis comparing the age-corrected anterior chamber depth with the ground truth group for male Asians for each of the regression analyses (sixth-, fifth-, fourth-, third- and second-order polynomial and linear), depicted as per Supplementary Figure 1.

Figure S4. Bland-Altman analysis comparing the age-corrected anterior chamber depth with the ground truth group for female Asians for each of the regression analyses (sixth-, fifth-, fourth-, third- and second-order polynomial and linear), depicted as per Supplementary Figure 1.

Figure S5. Analysis of age-related changes (top), distributions of age-corrected chamber depth (middle) and Bland-Altman comparison of age-corrected depths against the ground truth 30-40 year old cohort (bottom) for the refraction-corrected male Caucasian group.

Figure S6. Analysis of age-related changes (top), distributions of age-corrected chamber depth (middle) and Bland-Altman comparison of age-corrected depths against the ground truth 30-40 year old cohort (bottom) for the refraction-corrected male Asian group, depicted as per Supplementary Figure 5.

Figure S7. Analysis of age-related changes (top), distributions of age-corrected chamber depth (middle) and

Bland-Altman comparison of age-corrected depths against the ground truth 30-40 year old cohort (bottom) for the refraction-corrected female Asian group, depicted as per Supplementary Figure 6.

Table S1. All regression fits (linear, centred second- to sixth-order polynomial) for the male Caucasian cohort. Groups 1-7 refer to Figure 1.

Table S2. All regression fits (linear, centred second- to sixth-order polynomial) for the female Caucasian cohort. Groups 1-7 refer to Figure 1.

Table S3. All regression fits (linear, centred second- to sixth-order polynomial) for the male Asian cohort. Groups 1-7 refer to Figure 1.

Table S4. All regression fits (linear, centred second- to sixth-order polynomial) for the female Asian cohort. Groups 1-7 refer to Figure 1.

Table S5. Best-fit polynomial functions for each cohort divided by each of the six or seven clusters from hierarchical cluster analysis following initial refractive correction (Supplementary Figures 1-4).

Table S6. Mean, standard deviation (SD) and calculated 95% distribution limits of anterior chamber depths across each age-corrected and refractive-corrected group for each gender and ethnicity cohort.